

Distributed Robust Optimal Dispatch of Regional Integrated Energy Systems Based on ADMM Algorithm with Adaptive Step Size

Zhoujun Ma, Yizhou Zhou, Yuping Zheng, Li Yang, and Zhinong Wei

Abstract—This paper proposes a distributed robust optimal dispatch model to enhance information security and interaction among the operators in the regional integrated energy system (RIES). Our model regards the distribution network and each energy hub (EH) as independent operators and employs robust optimization to improve operational security caused by wind and photovoltaic (PV) power output uncertainties, with only deterministic information exchanged across boundaries. This paper also adopts the alternating direction method of multipliers (ADMM) algorithm to facilitate secure information interaction among multiple RIES operators, maximizing the benefit for each subject. Furthermore, the traditional ADMM algorithm with fixed step size is modified to be adaptive, addressing issues of redundant interactions caused by suboptimal initial step size settings. A case study validates the effectiveness of the proposed model, demonstrating the superiority of the ADMM algorithm with adaptive step size and the economic benefits of the distributed robust optimal dispatch model over the distributed stochastic optimal dispatch model.

Index Terms—Regional integrated energy system (RIES), distributed optimization, robust optimization, operation security, energy hub (EH).

I. INTRODUCTION

WITH escalating energy demands and pressing environmental challenges, research on integrated energy systems (IESs) has gained prominence [1]. IES can potentially overcome the limitations of independent operation among diverse energy systems, significantly enhancing energy efficiency and facilitating the integration of renewable energy sources (RESs) into the grid [2], [3]. Regional integrated energy systems (RIESs) are rapidly advancing in countries

such as the United States [4], [5], Europe [6], and China [7], with several ongoing projects. Unlike IESs for the transmission network, RIES features the energy hub (EH) as the coupler for energy production, storage, conversion, and distribution.

With the large-scale integration of RESs and distributed energy sources such as distributed energy storage into the grid, the architecture and operation of RIESs are growing increasingly complex. Consequently, centralized dispatch systems introduce vulnerabilities in safeguarding operators' information privacy due to their high communication demands. Therefore, the security and stability of RIES' operation are not guaranteed. Moreover, the centralized dispatch amplifies operational uncertainties stemming from variations in wind and photovoltaic (PV) power outputs across the entire system, transforming local risks into global ones and undermining the original objective of achieving efficient and stable RIES operation.

Determining a suitable distributed algorithm that addresses information security concerns among operators and mitigates uncertainty caused by fluctuations in the wind and PV power outputs is crucial, which represents the primary focus of our research.

Uncertainties within RIES primarily arise from distributed clean energy outputs [8]–[10], electricity/gas/heat load fluctuations [11]–[13], and energy prices [14]. These uncertainties are tackled using robust optimization [15], [16], stochastic optimization [17], [18], and chance-constrained optimization [19]. Reference [20] developed an optimization model for RIES, encompassing power supply, heating, and cooling considering energy price responsiveness, and reducing optimizing cost while minimizing environmental impact. In addition to demand response, [21] considered the influence of carbon abatement costs on RIES operation, while [22] proposed a mixed-integer linear optimization model to simulate an integrated power and heating system with renewable energy integration. Their findings highlighted the effectiveness of electric boilers (EBs) in mitigating wind power curtailment. For the RIES featuring an EH as the coupler, [23] proposed a regional integrated energy system security region (RIESSR) model based on the $N-1$ security guideline. Reference [24] developed an economic dispatch model for RIES, incorporating the ladder carbon trading mechanism and the fruit fly optimization algorithm (FOA) to obtain optimized EH opera-

Manuscript received: April 1, 2023; revised: June 15, 2023; accepted: August 26, 2023. Date of CrossCheck: August 26, 2023. Date of online publication: October 13, 2023.

This work was supported in part by the National Natural Science Foundation of China (No. 52107085) and the Natural Science Foundation of Jiangsu Province (No. BK20210367).

This article is distributed under the terms of the Creative Commons Attribution 4.0 International License (<http://creativecommons.org/licenses/by/4.0/>).

Z. Ma, Y. Zhou, Y. Zheng (corresponding author), L. Yang, and Z. Wei are with the College of Energy and Electrical Engineering, Hohai University, Nanjing 211100, China, Z. Ma is also with State Grid Jiangsu Electric Power Co., Ltd., Nanjing 210019, China, and Y. Zheng is also with State Key Laboratory of Smart Grid Protection and Control, NARI Group Corporation, Nanjing 211106, China (e-mail: mazhoujunsgecc@163.com; yizhou@hhu.edu.cn; zhengyuping@sgepri.sgcc.com.cn; hhuyangli@hhu.edu.cn; wzn_nj@263.net).

DOI: 10.35833/MPCE.2023.000204



tion strategies. Reference [25] designed a distributed robust optimization model for the resilient operation of the integrated electricity and heat energy distribution systems under extreme weather conditions. Reference [26] implemented the column-and-constraint generation (CCG) method to solve the two-stage robust model to advance the accommodation of renewable energy.

IES transcends the limitations of single energy sources and features the coupling of various energy systems using the coupler. While most existing research on IES operational models focuses on centralized dispatch [27], practical IES deployments involve multiple stakeholders or operators [28]. Reference [29] introduced a distributed optimization approach based on neurodynamics to facilitate the incorporation of intermittent renewable sources. Reference [30] developed a Stackelberg model with the IES operator as the leader and prosumers as the followers, respectively, guiding the merging of the energy sharing economy and IES. Reference [31] explored the integrated electricity and hydrogen energy sharing mechanism and utilized distributed optimization techniques to solve the model. Among the various distributed optimization algorithms, the alternating direction method of multipliers (ADMM) algorithm finds frequent applications [32]-[35]. Reference [32] utilized the ADMM algorithm with the RIES operator as an intermediary to facilitate energy sharing between the multi-energy complementary microgrids (MECMs) and the main grid. In addition, their study demonstrated the effectiveness of the ADMM in the distributed optimization of energy sharing while preserving the interests and privacy of the MECM operators within the electricity market. Reference [33] investigated the decentralized demand management, casting users as central players in the industrial park, and compared it with a centralized approach. Reference [34] examined a two-stage robust model for multi-regional integrated electricity-gas systems. After convexification with linearization, this model efficiently addressed the locational marginal price (LMP) based market clearing issue. Reference [35] introduced a two-stage distributionally robust optimization model, with high solution efficiency and low decision-making conservatism. Reference [36] presented a tri-level data-driven hybrid approach, amalgamating the strengths of stochastic and robust optimization.

Although optimization operations of RIESs have substantially progressed, several significant shortcomings in this domain exist. First, the predominant research focus of RIES operation is on centralized dispatch, with distributed dispatch occasionally considered, albeit primarily from a disparate regional or user-centric perspective. However, the distributed operation of RIESs and EHs remains underexplored. Second, most studies consider the operational uncertainties of the wind and PV power outputs of RIESs from the overall perspective overlooking local level uncertainties. Finally, the ADMM algorithm is often applied in distributed optimization research [37]; however, challenges such as suboptimal initial iteration step size settings continue to impede computational efficiency.

Therefore, we propose an optimal dispatch model for the RIES, where energy sources encompassing electricity, gas,

and heating are integrated, while the distribution network and EHs operate independently for distributed operations. The main contributions of this paper are as follows:

1) A distributed robust optimal dispatch model for RIESs is proposed, where the distribution network and EHs operate autonomously, optimizing dispatch and decision-making without compromising the system's overall integrity while preserving operator privacy.

2) The ADMM algorithm is optimized by substituting the fixed step size with an adaptive one, reducing iteration counts and the computation time. This approach mitigates the impact of arbitrary step size settings on computational efficiency.

The remainder of this paper is organized as follows. Section II presents the stochastic optimal dispatch model of RIESs. Section III proposes the distributed robust optimal dispatch model of RIESs. Section IV illustrates and discusses numerical simulation results from a case study. Section V outlines the findings of this paper.

II. STOCHASTIC OPTIMAL DISPATCH MODEL OF RIESs

This section presents a stochastic optimal dispatch model of RIESs that considers the uncertainty of renewable energy output.

A. Objective

We construct a centralized optimization model for the EH and electricity-gas-heat IES to minimize the day-ahead dispatch cost of the system. The cost encompasses expenses related to electricity and gas procurement, penalties associated with wind and PV power curtailment, and costs of pollutant emissions. The objective function is expressed as:

$$\min \sum_s \rho_s \left\{ \sum_t \left(C_{buy,t} P_{buy,t}^s + C_{gas,t} F_{S,m}^{s,t} + C_{pv,t} \Delta P_{pv,t}^s + C_{w,t} \Delta P_{w,t}^s \right) + \sum_t \sum_k \sum_b \left[P_{eb,k}^{s,t} Q_{eb,b}^{s,t} (V_{eb,b} + Y_{eb,b}) + H_{gas} F_{htg,k}^{s,t} Q_{chp,b}^{s,t} (V_{chp,b} + Y_{chp,b}) \right] \right\} \quad (1)$$

where s denotes the scenario number; t represents the time period number; k is the EH number; ρ_s is the probability of each scenario; $C_{buy,t}$ and $C_{gas,t}$ are the unit electricity and gas purchase costs, respectively; $P_{buy,t}^s$ is the active power purchased from the grid; $F_{S,m}^{s,t}$ is the gas supply at the gas source; $C_{pv,t}$ and $C_{w,t}$ are the penalty costs of PV and wind power curtailments, respectively; $\Delta P_{pv,t}^s$ and $\Delta P_{w,t}^s$ are the PV and wind power curtailments, respectively; H_{gas} is the calorific value of natural gas; $F_{htg,k}^{s,t}$ is the natural gas flow consumed by combined heat and power (CHP) unit; $P_{eb,k}^{s,t}$ is the electric power consumed by EBs; $Q_{chp,b}^{s,t}$ and $Q_{eb,b}^{s,t}$ are the emissions of the b^{th} pollutant of the CHP unit and EB, respectively; $V_{chp,b}$ and $Y_{chp,b}$ are the environmental value and penalty of the b^{th} pollutant of the CHP unit, respectively; and $V_{eb,b}$ and $Y_{eb,b}$ are the environmental value and penalty of the b^{th} pollutant of the EB, respectively.

B. Power Distribution Network (PDN) Operation Constraints

We establish the PDN with a radial topology, employing

the linear Dist-Flow model [38] as:

$$P_{ij,t}^s = \sum_{r \in j} P_{jr,t}^s - P_{j,t}^{s,t} + P_{eth,i}^t + P_{buy,t}^s \quad (2)$$

$$Q_{ij,t}^s = \sum_{r \in j} Q_{jr,t}^s + Q_{j,MT}^{s,t} - Q_{j,L}^{s,t} + Q_{buy,t}^s \quad (3)$$

$$U_{i,t}^s - U_{j,t}^s = (P_{ij,t}^s r_{ij} + Q_{ij,t}^s x_{ij}) / U_{0,t}^s \quad (4)$$

$$P_{buy}^{\min} \leq P_{buy,t}^s \leq P_{buy}^{\max} \quad (5)$$

$$U^{\min} \leq U_{i,t}^s \leq U^{\max} \quad (6)$$

$$P_{ij}^{\min} \leq P_{ij,t}^s \leq P_{ij}^{\max} \quad (7)$$

$$Q_{ij}^{\min} \leq Q_{ij,t}^s \leq Q_{ij}^{\max} \quad (8)$$

where $P_{ij,t}^s$ and $Q_{ij,t}^s$ are the active and reactive transmission power from node i to j , respectively; $P_{j,L}^{s,t}$ and $P_{eth,i}^t$ are the load power and EH interaction power, respectively, where the information on EH interaction power is deterministic and does not incorporate the scenario dimension in this paper; $Q_{j,MT}^{s,t}$ is the reactive power of micro-turbines; $Q_{j,L}^{s,t}$ and $Q_{buy,t}^s$ are the load power at node j and the reactive power purchased from the upper grid, respectively; $U_{i,t}^s$ and $U_{0,t}^s$ are the voltage and reference voltage, respectively; r_{ij} and x_{ij} are the resistance and reactance of transmission line (i, j) , respectively; P_{buy}^{\max} and P_{buy}^{\min} are the upper and lower limits of the electric power, respectively; U^{\max} and U^{\min} are the upper and lower limits of the nodal voltage amplitude, respectively; P_{ij}^{\max} and P_{ij}^{\min} are the upper and lower limits of the active transmission power of transmission line (i, j) , respectively; and Q_{ij}^{\max} and Q_{ij}^{\min} are the upper and lower limits of the reactive transmission power of transmission line (i, j) , respectively.

Constraints (2) and (3) represent the nodal active and reactive power balances, respectively. Constraint (4) denotes the nodal voltage drop equation. Constraint (5) sets the upper and lower limit of the power purchased from the upper grid, while constraint (6) represents that of the nodal voltage amplitude. Finally, constraints (7) and (8) signify the transmission power of transmission line.

C. Gas Distribution Network (GDN) Operation Constraints

Similar to the PDN, the GDN adheres to the topological principles, characterized by its radial, branching, or mesh structure during design and construction. The GDN model can be expressed as [39]:

$$F_{S,m}^{s,t} - F_{gh,m}^t = \sum_{n \in m} F_{mn,t}^s \quad (9)$$

$$(F_{mn,t}^s)^2 = C_{mn}^2 (\Pi_{m,t}^s - \Pi_{n,t}^s) \quad (10)$$

$$\Pi_m^{\min} \leq \Pi_{m,t}^s \leq \Pi_m^{\max} \quad (11)$$

$$F_S^{\min} \leq F_{S,m}^{s,t} \leq F_S^{\max} \quad (12)$$

$$F_{ramp}^{\min} \leq F_{S,m}^{s,t} - F_{S,m}^{s,t-1} \leq F_{ramp}^{\max} \quad (13)$$

where $F_{gh,m}^t$ is the deterministic natural gas consumption of the CHP unit; $F_{mn,t}^s$ is the pipe flow of pipeline mn ; C_{mn} is the Wey-mouth constant of pipeline mn ; $\Pi_{m,t}^s$ is the square of the nodal air pressure; Π_m^{\max} and Π_m^{\min} are the upper and lower

limits for the square of nodal air pressure, respectively; F_S^{\max} and F_S^{\min} are the upper and lower limits of the gas supply at the gas source, respectively; and F_{ramp}^{\max} and F_{ramp}^{\min} are the upper and lower limits of the ramp rate at the gas source, respectively.

Constraint (9) represents the nodal flow balance. Constraint (10) depicts the relationship between pipe flow and nodal air pressure at both ends. Constraint (11) represents the upper and lower limits of the square of the nodal air pressure, while constraint (12) represents that of the gas supply at the gas source. Constraint (13) governs the ramp rate at the gas source.

The non-convex relationship between pipe flow and nodal air pressure (constraint (10)) can be convexified using second-order cone (SOC) relaxation, resulting in constraint (14), whose standard representation is illustrated in constraint (15). The relaxation of the non-convex constraint into a convex one facilitates determining the global optimal solution and enhances solution efficiency.

$$(F_{mn,t}^s)^2 \leq C_{mn}^2 (\Pi_{m,t}^s - \Pi_{n,t}^s) \Rightarrow (2F_{mn,t}^s / C_{mn})^2 + (\Pi_{m,t}^s - \Pi_{n,t}^s - 1)^2 \leq (\Pi_{m,t}^s - \Pi_{n,t}^s + 1)^2 \quad (14)$$

$$\left\| \frac{2F_{mn,t}^s / C_{mn}}{\Pi_{m,t}^s - \Pi_{n,t}^s - 1} \right\| \leq \Pi_{m,t}^s - \Pi_{n,t}^s + 1 \quad (15)$$

D. Thermal Distribution Network (TDN) Operation Constraint

The TDN model is non-linear and non-convex, which is difficult to solve. Consequently, we adopt the widely used quality regulation model to characterize the TDN [40]. This model comprises the pipeline loss constraint (16), the nodal flow balance constraint (17), the nodal power balance constraint (18), the nodal temperature constraint (19), the user power constraint (20), and the heat source power constraint (21).

$$T_{ed,v}^{s,t} = (T_{st,u}^{s,t} - T_{a,t}^s) e^{-\frac{L_{uv}}{Rcpf_w}} + T_{a,t}^s \quad (16)$$

$$\sum_{u \in v} f_{uv}^s = \sum_{w \in v} f_{vw}^s \quad (17)$$

$$\sum_{u \in v} T_{ed,v}^{s,t} f_{uv}^s = T_{st,v}^{s,t} \sum_{w \in v} f_{vw}^s \quad (18)$$

$$T_{st,v}^{s,t} = T_{v,t}^s \quad (19)$$

$$H_{l,t}^s = c\rho\eta f_l^s (T_{LS,t}^s - T_{LR,t}^s) \quad (20)$$

$$H_{S,t}^s = c\rho\eta f_S^s (T_{HS,t}^s - T_{HR,t}^s) \quad (21)$$

where u , v , and w denote the TDN node numbers; $T_{st,u}^{s,t}$ and $T_{ed,v}^{s,t}$ are the temperatures of the pipeline uv at its start and end, respectively; $T_{a,t}^s$ and $T_{v,t}^s$ are the ambient and node temperatures, respectively; f_{uv}^s , f_l^s , and f_S^s are the pipe flows of the pipeline, load, and heat source, respectively; R is the specific thermal resistance of the pipeline; c is the specific heat capacity of water; L_{uv} is the pipe length; η is the efficiency of the heat exchanger; $H_{l,t}^s$ and $H_{S,t}^s$ are the power of the load and heat source, respectively; $T_{LS,t}^s$

and $T_{LR,t}^s$ are the supply and return water temperatures of the load, respectively; and $T_{HS,t}^s$ and $T_{HR,t}^s$ are the supply and return water temperatures of the heat source, respectively.

The TDN model must adhere to the constraints of node temperature (22), supply and return water temperatures of the load (23) and (25), and supply and return water temperatures of the heat source (24) and (26) during the operation.

$$T_{v,t}^{\min} \leq T_{v,t}^s \leq T_{v,t}^{\max} \quad (22)$$

$$T_{LS,t}^{\min} \leq T_{LS,t}^s \leq T_{LS,t}^{\max} \quad (23)$$

$$T_{HS,t}^{\min} \leq T_{HS,t}^s \leq T_{HS,t}^{\max} \quad (24)$$

$$T_{LR,t}^{\min} \leq T_{LR,t}^s \leq T_{LR,t}^{\max} \quad (25)$$

$$T_{HR,t}^{\min} \leq T_{HR,t}^s \leq T_{HR,t}^{\max} \quad (26)$$

where $T_{v,t}^{\max}$ and $T_{v,t}^{\min}$ are the upper and lower limits of the node temperature, respectively; $T_{LS,t}^{\max}$ and $T_{LS,t}^{\min}$ are the upper and lower limits of the supply water temperature of the load, respectively; $T_{HS,t}^{\max}$ and $T_{HS,t}^{\min}$ are the upper and lower limits of the return water temperature of the heat source, respectively; $T_{LR,t}^{\max}$ and $T_{LR,t}^{\min}$ are the upper and lower limits of the return water temperature of the load, respectively; and $T_{HR,t}^{\max}$ and $T_{HR,t}^{\min}$ are the upper and lower limits of the return water temperature of the heat source, respectively.

E. EH Operation Constraints

The integration of PDN, GDN, and TDN should be considered in the electricity-gas-heat IES, therefore, we use the EH as the node for modeling. The EH is a coupled component with various energy inputs and outputs, encompassing electricity, heating, gas, and other energy sources through energy conversion and storage processes. The operation of the EH-based IES shown in Fig. 1 showcases diverse energy conversion pathways within the EH. In addition, with the given load, the operation of the EH can be optimized by adjusting the internal dispatch variables and energy inputs. Therefore, leveraging the EH model for energy coupling provides enhanced optimization opportunities and greater flexibility in multi-energy operations.

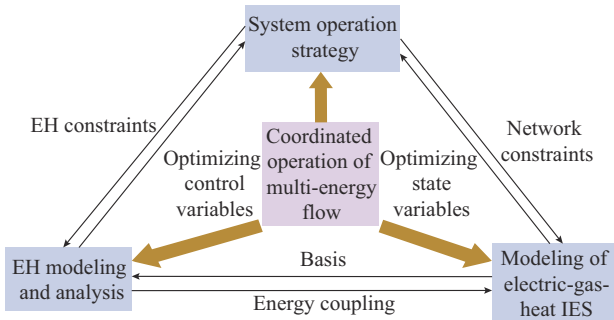


Fig. 1. Operation of EH-based IES.

The electricity-gas-heat IES establishes connections between the PDN, GDN, and TDN through EH. The structure of the EH is shown in Fig. 2, which consists of RES, CHP unit, EB, electric energy storage (EES), and thermal energy storage (TES). The electric and gas power is on the input side, while the electric and heat power is on the output

side.

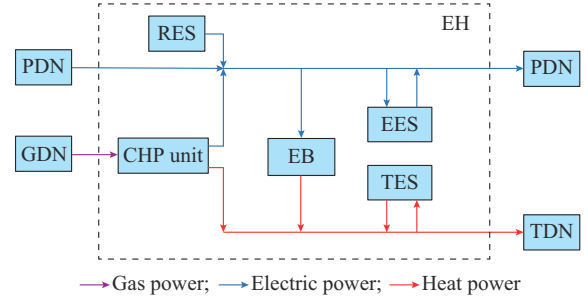


Fig. 2. Structure of EH.

CHP unit generates electric energy by utilizing natural gas, which is transformed into heat energy limited by gas power constraints (27)-(30). Constraint (29) represents climbing constraint of the CHP unit, indicating its ability supporting rapid changes. EBs convert electric energy into heat energy. The electro-heat conversion equation of EBs is presented in (31), and electric power consumption constraints of EBs are denoted in (32) and (33). During the EES operation, the equations of power balance and the constraints of energy storage capacity, charging power, and discharging power are illustrated in (34)-(38), while those during the TES operation are illustrated in (39)-(43).

$$P_{chp,k,e}^{s,t} = \eta_{chp,k,e} H_{gas} F_{htg,k}^{s,t} \quad (27)$$

$$H_{chp,k,h}^{s,t} = \eta_{chp,k,h} H_{gas} F_{htg,k}^{s,t} \quad (28)$$

$$-R_{chp,t}^d \Delta t \leq P_{chp,k,e}^{s,t+1} - P_{chp,k,e}^{s,t} \leq R_{chp,t}^u \Delta t \quad (29)$$

$$F_{htg,k}^{\min} \leq F_{htg,k}^t \leq F_{htg,k}^{\max} \quad (30)$$

$$H_{eb,k}^{s,t} = \eta_{eb,k} P_{eb,k}^{s,t} \quad (31)$$

$$-R_{eb,t}^d \Delta t \leq H_{eb,k}^{s,t+1} - H_{eb,k}^{s,t} \leq R_{eb,t}^u \Delta t \quad (32)$$

$$P_{eb,k}^{\min} \leq P_{eb,k}^{s,t} \leq P_{eb,k}^{\max} \quad (33)$$

$$E_{e,k}^{s,t} = E_{e,k}^{s,t-1} + \left(P_{k,ch}^{s,t-1} \eta_{e,k}^{ch} - P_{k,dis}^{s,t-1} / \eta_{e,k}^{dis} \right) \Delta t \quad (34)$$

$$E_{e,k}^{s,t=0} = E_{e,k}^{s,t=T} \quad (35)$$

$$E_{e,k}^{\min} \leq E_{e,k}^{s,t} \leq E_{e,k}^{\max} \quad (36)$$

$$0 \leq P_{k,ch}^{s,t} \leq P_{k,ch}^{\max} \quad (37)$$

$$0 \leq P_{k,dis}^{s,t} \leq P_{k,dis}^{\max} \quad (38)$$

$$E_{h,k}^{s,t} = E_{h,k}^{s,t-1} + \left(H_{k,ch}^{s,t-1} \eta_{h,k}^{ch} - H_{k,dis}^{s,t-1} / \eta_{h,k}^{dis} \right) \Delta t \quad (39)$$

$$E_{h,k}^{s,t=0} = E_{h,k}^{s,t=T} \quad (40)$$

$$E_{h,k}^{\min} \leq E_{h,k}^{s,t} \leq E_{h,k}^{\max} \quad (41)$$

$$0 \leq H_{k,ch}^{s,t} \leq H_{k,ch}^{\max} \quad (42)$$

$$0 \leq H_{k,dis}^{s,t} \leq H_{k,dis}^{\max} \quad (43)$$

where $\eta_{chp,k,e}$ and $\eta_{chp,k,h}$ are the efficiencies of CHP units that convert natural gas to electric and heat power, respectively; $P_{chp,k,e}^{s,t}$ and $H_{chp,k,h}^{s,t}$ are the electric and heat power generated by CHP units, respectively; $R_{chp,t}^u$ and $R_{chp,t}^d$ are the upper and lower limits of the ramp rate of CHP units, respectively; $F_{htg,k}^{\max}$ and $F_{htg,k}^{\min}$ are the upper and lower limits of gas

power consumption, respectively; $\eta_{eb,k}$ is the conversion efficiency of EB; $H_{eb,k}^{s,t}$ is the heat power of EB; $R_{eb,t}^u$ and $R_{eb,t}^d$ are the upper and lower limits of the ramp rate of CHP units, respectively; $P_{eb,k}^{\max}$ and $P_{eb,k}^{\min}$ are the upper and lower limits of electric power consumption, respectively; $E_{e,k}^{s,t=0}$, $E_{e,k}^{s,t=T}$, and $E_{e,k}^t$ are the EES capacities in the period t , initial period, and end period, respectively; $E_{e,k}^{\max}$ and $E_{e,k}^{\min}$ are the upper and lower limits of EES capacity, respectively; $\eta_{e,k}^{ch}$ and $\eta_{e,k}^{dis}$ are the charging and discharging efficiencies of EES, respectively; $P_{k,ch}^{s,t}$ and $P_{k,dis}^{s,t}$ are the charging and discharging power of EES, respectively; $P_{k,ch}^{\max}$ and $P_{k,dis}^{\max}$ are the upper limits of the charging and discharging power of EES, respectively; $E_{h,k}^{s,t=0}$, $E_{h,k}^{s,t=T}$, and $E_{h,k}^t$ are the TES capacities in the period t , initial period, and end period, respectively; $E_{h,k}^{\max}$ and $E_{h,k}^{\min}$ are the upper and lower limits of TES capacity, respectively; $\eta_{h,k}^{ch}$ and $\eta_{h,k}^{dis}$ are the charging and discharging efficiencies of TES, respectively; $H_{k,ch}^{s,t}$ and $H_{k,dis}^{s,t}$ are the charging and discharging power of TES, respectively; and $H_{k,ch}^{\max}$ and $H_{k,dis}^{\max}$ are the upper limits of charging and discharging power of TES, respectively.

Constraints (44) and (45) correspond to the electric energy balance equation and heat energy balance equation during the operation of EH.

$$P_{PV,k}^{s,t} + P_{WT,k}^{s,t} + P_{chp,k,e}^{s,t} - P_{k,ch}^{s,t} + P_{k,dis}^{s,t} - P_{eb,k}^{s,t} = P_{hte,k}^t \quad (44)$$

$$H_{chp,k,h}^{s,t} + H_{eb,k}^{s,t} - H_{k,ch}^{s,t} + H_{k,dis}^{s,t} = H_{hth,k}^t \quad (45)$$

where $P_{PV,k}^{s,t}$ and $P_{WT,k}^{s,t}$ are the generated PV power and wind power in the EH, respectively; and $P_{hte,k}^t$ and $H_{hth,k}^t$ are the deterministic interactive power between the EH and PDN and between the EH and TDN, respectively.

III. DISTRIBUTED ROBUST OPTIMAL DISPATCH MODEL OF RIESS

A. ADMM Algorithm with Adaptive Step Size

The concept of ADMM algorithm was first proposed in [41] and was systematically developed into a comprehensive theory in the mid-1990s. The ADMM algorithm, employing decomposition coordination, offers an effective solution for distributed convex optimization problems by combining dual decomposition and the augmented Lagrangian method in constraint optimization. ADMM algorithm also coordinates the solutions of the local problems to yield that of the global problem [42]. ADMM algorithm is widely implemented in various domains, including engineering design, multi-period investment portfolio optimization, and time series analysis and dispatch. Due to its strong robustness and convergence, ADMM algorithm is well suited for solving complex problems such as constraint (46).

$$\begin{cases} \min (f(\mathbf{x}) + g(\mathbf{z})) \\ \text{s.t. } \mathbf{Ax} + \mathbf{Bz} = \mathbf{c} \end{cases} \quad (46)$$

where $f(\mathbf{x})$ and $g(\mathbf{z})$ are the objective functions of two different subproblems; $\mathbf{A} \in \mathbf{R}^{p \times n}$, $\mathbf{B} \in \mathbf{R}^{p \times m}$, and $\mathbf{c} \in \mathbf{R}^p$ are the coupling coefficient matrices between the variables; and $\mathbf{x} \in \mathbf{R}^n$ and $\mathbf{z} \in \mathbf{R}^m$ are the coupling variables between the two subproblems.

The ADMM algorithm allows the incorporation of the coupling variable constraints to the objective function (46) to ac-

quire its augmented Lagrangian function:

$$L_\rho(\mathbf{x}, \mathbf{z}, \boldsymbol{\lambda}) = f(\mathbf{x}) + g(\mathbf{z}) + \boldsymbol{\lambda}^T (\mathbf{Ax} + \mathbf{Bz} - \mathbf{c}) + \frac{\rho}{2} \|\mathbf{Ax} + \mathbf{Bz} - \mathbf{c}\|^2 \quad (47)$$

where $L_\rho(\mathbf{x}, \mathbf{z}, \boldsymbol{\lambda})$ is the augmented Lagrangian function; $\boldsymbol{\lambda}^T$ is the dual variable; and ρ is the step size, $\rho > 0$.

Iterative solutions of two RIESSs in different regions are detailed as:

$$\mathbf{x}^{\alpha+1} = \arg \min_{\mathbf{x}} L_\rho(\mathbf{x}, \mathbf{z}^\alpha, \boldsymbol{\lambda}^\alpha) \quad (48)$$

$$\mathbf{z}^{\alpha+1} = \arg \min_{\mathbf{z}} L_\rho(\mathbf{x}^{\alpha+1}, \mathbf{z}, \boldsymbol{\lambda}^\alpha) \quad (49)$$

$$\boldsymbol{\lambda}^{\alpha+1} = \boldsymbol{\lambda}^\alpha + \rho (\mathbf{Ax}^{\alpha+1} + \mathbf{Bz}^{\alpha+1} - \mathbf{c}) \quad (50)$$

where α is the iteration number; $\mathbf{x}^{\alpha+1}$ and $\mathbf{z}^{\alpha+1}$ are the coupling variables obtained after the $(\alpha+1)^{\text{th}}$ iteration; and $\boldsymbol{\lambda}^{\alpha+1}$ is the dual variable obtained after the $(\alpha+1)^{\text{th}}$ iteration.

Optimization utilizing the standard ADMM algorithm involves an iterative process between two regions performed alternately in a predetermined orders 1-4, as shown in Fig. 3. The updated optimization value of Region 1 is substituted into Region 2 to obtain the optimization solution. Once all regions have undergone this optimization process, global iteration variables are updated and broadcast via the coordination center.

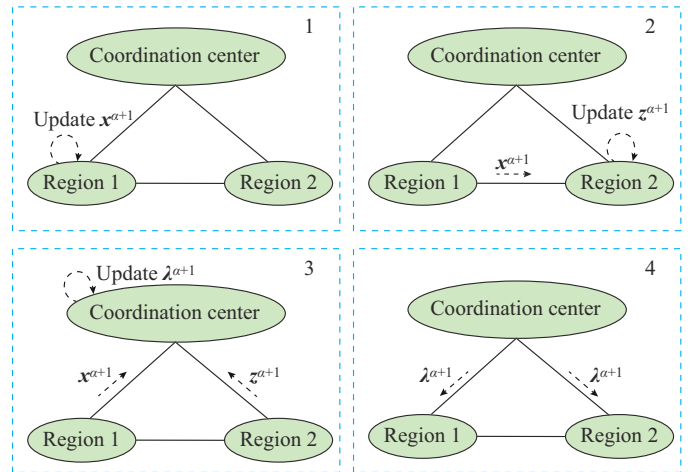


Fig. 3. Optimization of two regions with standard ADMM algorithm.

The iteration process terminates when the original and dual residuals are below the minimal value, denoted as:

$$\begin{cases} \|\mathbf{r}^{\alpha+1}\|_2 \leq \varepsilon^{pri} \\ \|\mathbf{s}^{\alpha+1}\|_2 \leq \varepsilon^{dual} \end{cases} \quad (51)$$

$$\begin{cases} \mathbf{r}^{\alpha+1} = \mathbf{Ax}^{\alpha+1} + \mathbf{Bz}^{\alpha+1} - \mathbf{c} \\ \mathbf{s}^{\alpha+1} = \rho \mathbf{A}^T \mathbf{B} (\mathbf{z}^{\alpha+1} - \mathbf{z}^\alpha) \end{cases} \quad (52)$$

where $\mathbf{r}^{\alpha+1}$ and $\mathbf{s}^{\alpha+1}$ are the values of the original and dual residuals after the $(\alpha+1)^{\text{th}}$ iteration, respectively; and ε^{pri} and ε^{dual} are the upper tolerance limits of the original and dual residuals, respectively.

The choice of step size significantly impacts the calculation speed of the ADMM algorithm, thus the ADMM algo-

algorithm with adaptive step size is adopted in this paper. It can automatically update the step size based on the relative relationship between the original and dual residuals, as shown in (53). This approach enhances the convergence speed at the start of the iteration and mitigates oscillation toward the end, subsequently resulting in significant improvements in calculation speed.

$$\rho^{\alpha+1} = \begin{cases} \tau^{incr} \rho^{\alpha} & \|r^{\alpha}\|_2 > \mu \|s^{\alpha}\|_2 \\ \rho^{\alpha} / \tau^{decr} & \|s^{\alpha}\|_2 > \mu \|r^{\alpha}\|_2 \\ \rho^{\alpha} & \text{otherwise} \end{cases} \quad (53)$$

where $\mu > 1$ is the proportional coefficient between the original and dual residuals; and $\tau^{incr} > 1$ and $\tau^{decr} > 1$ are the acceleration and deceleration factors, respectively, which are used to increase and decrease the step size during the iteration. When the original residual increases, the step size is adjusted to modify the relationship between the coupling variables x and z , which will expedite the convergence of the original residual. When the dual residual increases, the step size is reduced to expedite the convergence of z and diminish the oscillation of the objective function.

B. Distributed Optimization Mechanism of RIESs

Although the PDN, GDN, and TDN largely maintain independent operation, notable progress is being made in some domains [43]. Referring to energy station operators of park type and layer scheduling departments of regional distribution network, this paper considers each EH and RIES operator as a separate entity.

The distributed optimization framework of the electricity-gas-heat IES with multiple EHs is depicted in Fig. 4. First, the optimization model for IES and EH is developed to minimize the system operation cost. The RIES operator manages the PDN, GDN, and TDN, while EH operators manage their respective EHs. It should be noted that the resolution of uncertainty for each subject occurs internally, and the energy flow information between the RIES and EHs is deterministic, devoid of scenario information.

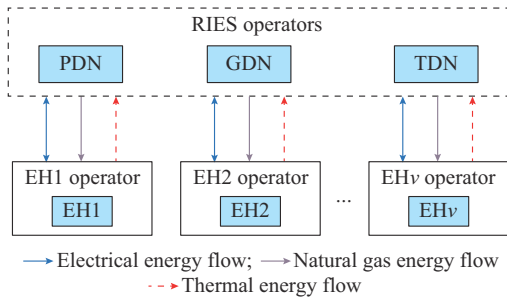


Fig. 4. Distributed optimization framework of electricity-gas-heat IES with multiple EHs.

Constraints (54)-(56) must be satisfied to achieve the distributed optimal operation of EHs in the IES. Constraint (54) represents that the interactive electric power injected in the PDN $P_{eth,k}^{s,t}$ is equal to that exported from the EH $P_{hte,k}^{s,t}$. Constraint (55) represents that the interactive heat power injected in the TDN $H_{S,t}^s$ is equal to that exported from the EH $H_{htg,k}^{s,t}$. Constraint (56) denotes that the interactive gas power

exported from the TDN $F_{gth,k}^{s,t}$ is equal to that injected in the EH $F_{htg,k}^{s,t}$.

$$P_{eth,k}^{s,t} = P_{hte,k}^{s,t} \quad (54)$$

$$H_{S,t}^s = H_{htg,k}^{s,t} \quad (55)$$

$$F_{gth,k}^{s,t} = F_{htg,k}^{s,t} \quad (56)$$

C. Solution to Bi-level Robust Optimization Model

Stochastic optimization techniques often rely on assumptions regarding specific probability distribution for handling uncertainties. However, accurately determining these probability distributions of random variables can be challenging. Robust optimization closely considers the worst-case scenarios during the optimization process, potentially yielding overly conservative outcomes. In contrast, the distributed robust approach leverages statistical characteristics for decision-making, avoiding high costs associated with excessive conservatism while not necessitating accurate probability distributions.

The adoption of the distributed robust optimal dispatch model stabilizes system fluctuations caused by the randomness of wind and PV power outputs of EH, enhancing the safe operation of IES. The objective is to minimize the optimal dispatch cost of the IES in the worst-case scenarios.

$$\min \max_s \sum_t \left(C_{buy,t} P_{buy,t}^s + C_{gas,t} F_{S,m}^{s,t} + C_{pv,t} \Delta P_{pv,t}^s + C_{w,t} \Delta P_{w,t}^s \right) + \sum_t \sum_k \sum_b \left[P_{eb,k}^{s,t} Q_{eb,b}^{s,t} (V_{eb,b} + Y_{eb,b}) + H_{gas} F_{htg,k}^{s,t} Q_{chp,b}^{s,t} (V_{chp,b} + Y_{chp,b}) \right] \quad (57)$$

The objective function can be simplified as:

$$\min \max_s f(x, s) \quad (58)$$

where x denotes all the decision variables; and $f(x, s)$ denotes the cost function in each scenario.

The objective function (58) can be converted into (59) for the solution.

$$\begin{cases} \min y \\ \text{s.t. } y \geq f(x, s) \end{cases} \quad (59)$$

where y is the one-dimensional decision variable. The cost function in the worst-case scenario could be obtained through (59).

In this way, the bi-level robust optimization model could be converted to a single-level one to be solved.

D. Distributed Robust Optimization Model for RIES

Compared with stochastic optimization and robust optimization techniques, distributed robust optimization bridges the gap between data and decision-making, employing statistical and optimization frameworks. Additionally, it inherits the solvability of robust optimization and the flexibility of stochastic programming for characterizing stochastic problems. The distributed robust optimization employs the worst-case scenarios to regularize the optimization problem, thus alleviating the solution problem associated with the low efficiency of the optimizer in stochastic optimization.

In distributed optimization, the optimization of the electricity-gas-heat IES with multiple EHs can be decomposed into

the IES subproblems and k EH subproblems.

The augmented Lagrangian function of the IES subproblems is established as:

$$L_{ies}^s = \sum_t (C_{buy,t} P_{buy,t}^s + C_{gas,t} F_{S,m}^{s,t}) + \sum_t \sum_k \left[\lambda_{e,k}^{s,t,\alpha} (P_{eth,k}^{s,t} - P_{hte,k}^{s,t,\alpha}) + \lambda_{h,k}^{s,t,\alpha} (H_{S,t}^s - H_{hth,k}^{s,t,\alpha}) + \lambda_{g,k}^{s,t,\alpha} (F_{gth,k}^{s,t} - F_{hfg,k}^{s,t,\alpha}) + \frac{\rho_k^\alpha}{2} (P_{eth,k}^{s,t} - P_{hte,k}^{s,t,\alpha})^2 + \frac{\rho_k^\alpha}{2} (H_{S,t}^s - H_{hth,k}^{s,t,\alpha})^2 + \frac{\rho_k^\alpha}{2} (F_{gth,k}^{s,t} - F_{hfg,k}^{s,t,\alpha})^2 \right] \quad (60)$$

where $\lambda_{e,k}^{s,t,\alpha}$, $\lambda_{h,k}^{s,t,\alpha}$, and $\lambda_{g,k}^{s,t,\alpha}$ are the dual variables governing the consistency of the electric power between PDN and EH, the consistency of the heat power between TDN and EH, and the consistency of the gas power between the GDN and EH, respectively; and ρ_k^α is the step size in α iteration.

The augmented Lagrangian functions of the k EH subproblems are depicted as:

$$L_{eh,k}^s = \sum_t \left\{ (C_{pv,t} \Delta P_{pv,t}^s + C_{wt,t} \Delta P_{wt,t}^s) + \sum_k \sum_b \left[P_{eb,k}^{s,t} Q_{eb,b}^{s,t} (V_{eb,b} + Y_{eb,b}) + H_{gas} F_{hfg,k}^{s,t} Q_{chp,b}^{s,t} (V_{chp,b} + Y_{chp,b}) \right] + \lambda_{e,k}^{s,t,\alpha} (P_{eth,k}^{s,t,\alpha+1} - P_{hte,k}^{s,t}) + \lambda_{h,k}^{s,t,\alpha} (H_{S,t}^{s,\alpha+1} - H_{hth,k}^{s,t}) + \lambda_{g,k}^{s,t,\alpha} (F_{gth,k}^{s,t,\alpha} - F_{hfg,k}^{s,t}) + \frac{\rho_k^\alpha}{2} (P_{eth,k}^{s,t,\alpha+1} - P_{hte,k}^{s,t})^2 + \frac{\rho_k^\alpha}{2} (H_{S,t}^{s,\alpha+1} - H_{hth,k}^{s,t})^2 + \frac{\rho_k^\alpha}{2} (F_{gth,k}^{s,t,\alpha} - F_{hfg,k}^{s,t})^2 \right\} \quad (61)$$

The original and dual residuals should satisfy the stopping criteria as depicted in constraints (62) and (63), respectively.

$$\left[\sum_t \sum_k (P_{eth,k}^{s,t,\alpha+1} - P_{hte,k}^{s,t,\alpha+1})^2 + \sum_t \sum_k (H_{S,t}^{s,\alpha+1} - H_{hth,k}^{s,t,\alpha+1})^2 + \sum_t \sum_k (F_{gth,k}^{s,t,\alpha+1} - F_{hfg,k}^{s,t,\alpha+1})^2 \right]^{\frac{1}{2}} \leq \varepsilon^{pri} \quad (62)$$

$$\left[\sum_t \sum_k (\rho_k^{\alpha+1} (P_{hte,k}^{s,t,\alpha+1} - P_{hte,k}^{s,t,\alpha}))^2 + \sum_t \sum_k (\rho_k^{\alpha+1} (H_{hth,k}^{s,t,\alpha+1} - H_{hth,k}^{s,t,\alpha}))^2 + \sum_t \sum_k (\rho_k^{\alpha+1} (F_{hfg,k}^{s,t,\alpha+1} - F_{hfg,k}^{s,t,\alpha}))^2 \right]^{\frac{1}{2}} \leq \varepsilon^{dual} \quad (63)$$

In the final model, (57) represents the overall objective function, (60) and (61) denote the objective functions for each subject, and (2)-(9), (11)-(14), (16)-(45), (53)-(56), (62), and (63) are the constraints.

IV. CASE STUDY

A. Introduction

We validated the proposed model in an electricity-gas-heat IES, comprising a modified 33-node PDN, a 20-node GDN [44], a 32-node Barry Island TDN [45], and three EHs, as shown in Fig. 5. The PDN, GDN, and TDN have the maximum electricity, gas, and heat loads of (3.715 + j2.3) MVAh, 438.6 m³, and 2.164 MWh, respectively, in a single time period. The electricity, gas, and heat load curves are

shown in Fig. 6.

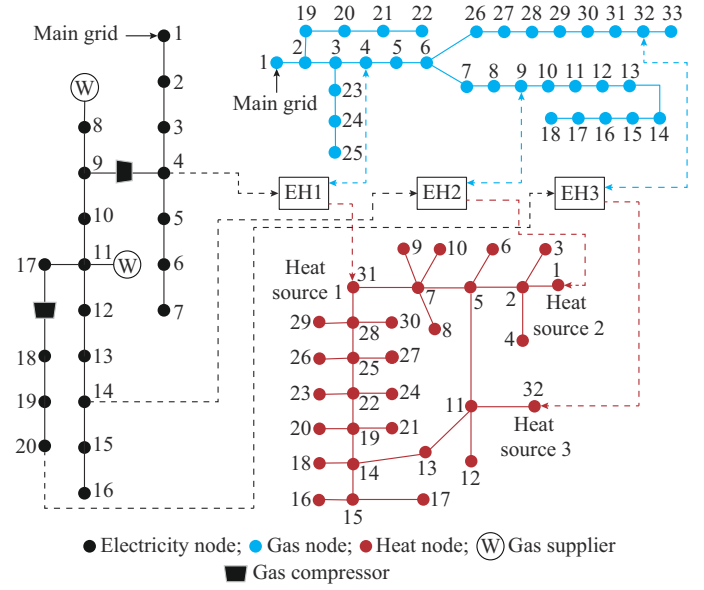


Fig. 5. Test system structure of electricity-gas-heat IES.

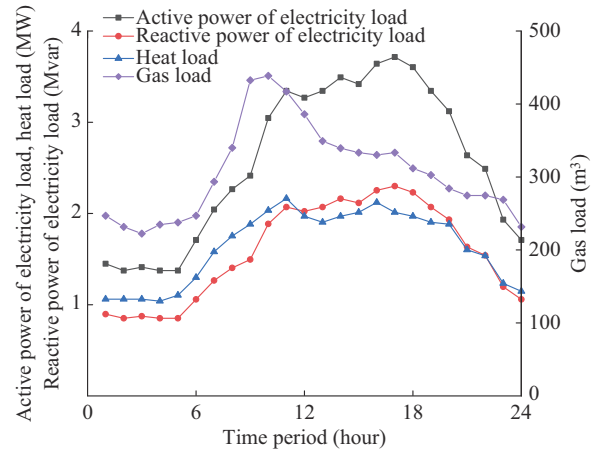


Fig. 6. Electricity, gas, and heat load curves.

Among the three EHs, EH1 installs PV units, EH2 installs wind turbines, and EH3 does not install any renewable energy unit. CHP units and EBs can each consume up to 1 MW/h of gas and electric power, respectively. The capacity of EES/TES is 1 MWh. The peak-valley time-of-use electricity price is used for purchasing from the upper grid, while the natural gas price is fixed at 3.45 ¥/m³, equivalent to a calorific value price of 0.349 ¥/kWh. Table I provides the electricity and gas prices, and Table II lists the parameters of equipment in EH. Based on historical data from a northwest Chinese city, the wind and PV power output scenarios [46] are reduced to 20 based on Monte Carlo method [47]. The reduced scenarios are shown in Figs. 7 and 8, where different colors represent wind and PV power outputs in different scenarios. The unit operation cost of CHP units, EBs, EES, and TES is 0.05 ¥/kWh. In the distributed optimization model, the upper tolerance limit for the original residual and dual residual is set to be 5×10^{-4} , μ is set to be 10, and τ^{decr} and τ^{incr} are set to be 2. We employ GAMS for programming,

and apply the GUROBI solver to address the SOC programming problem.

TABLE I
ELECTRICITY AND GAS PRICES

Period	Electricity price (¥/kWh)	Gas price (¥/kWh)
Peak period (12:00-14:00, 19:00-22:00)	1.188	0.349
Normal period (08:00-11:00, 15:00-18:00)	0.871	0.349
Valley period (01:00-07:00, 23:00-24:00)	0.475	0.349

TABLE II
PARAMETERS OF EQUIPMENT IN EH

Parameter	Value	Parameter	Value	Parameter	Value
$R_{chp,i}^u$	200 kW	$R_{chp,t}^d$	200 kW	$P_{eb,k}^{max}$	1000 kW
$R_{eb,i}^u$	200 kW	$R_{eb,t}^d$	200 kW	$E_{e,k,0}$	500 kWh
$E_{e,k}^{max}$	900 kWh	$E_{e,k}^{min}$	100 kWh	$P_{k,ch}^{max}$	300 kW
$P_{k,dis}^{max}$	300 kW	$E_{h,k,0}$	500 kWh	$E_{h,k}^{max}$	900 kWh
$E_{h,k}^{min}$	100 kWh	$H_{k,ch}^{max}$	300 kW	$H_{k,dis}^{max}$	300 kW
$\eta_{chp,k,e}$	35%	$\eta_{chp,k,h}$	45.5%	$\eta_{eb,k}$	90%
$\eta_{e,k}^{ch}$	95%	$\eta_{h,k}^{ch}$	95%		

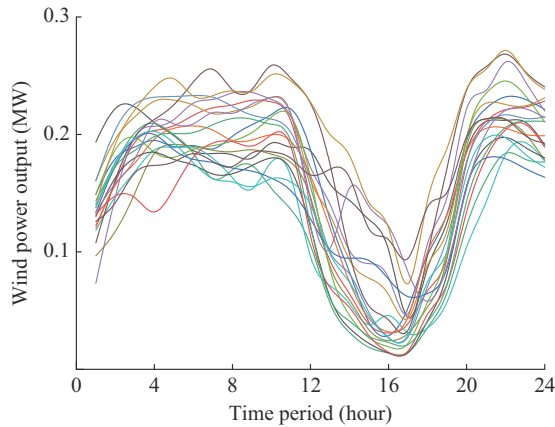


Fig. 7. Predicted wind power output curves.

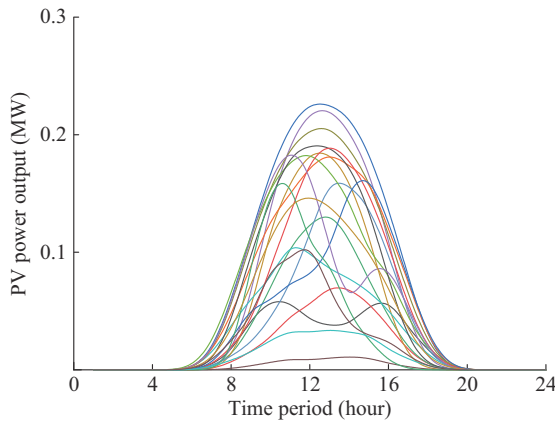


Fig. 8. Predicted PV power output curves.

The optimal dispatch results are acquired after solving the proposed model. The electric/heat power balance is analyzed

via the example of EH1 in Scenario 10, as shown in Fig. 9. Given the similar situation of EH2 and EH3, we refrain from reiterating the analyses of their electric/heat power balance in this paper. During off-peak hours (valley hours), EBs provide heat, causing CHP units to remain inactive during 01:00-07:00 and at 24:00. In contrast, in the normal and peak periods, CHP units are engaged for power and heat supplies. If excess PV cannot be accommodated in EH1, it can be fully consumed through the EB or directed to the distribution grid. The EES/TES is charged at a lower electricity purchase price and discharged at a higher price, enhancing the economy of the operation of the system.

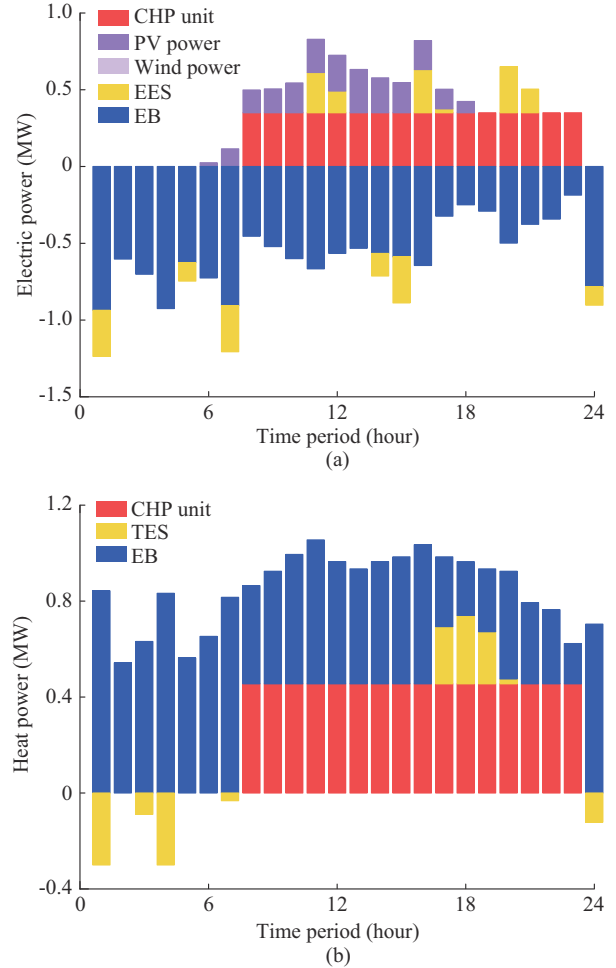


Fig. 9. Electric/heat power balance of EH1 in Scenario 10. (a) Electric power balance. (b) Heat power balance.

B. Economic Analysis of Distributed Robust Optimization Algorithm

Theoretically, distributed robust optimization promises the most robust operation strategy. This subsection compares and analyzes the results of distributed robust optimization and distributed stochastic optimization algorithms, as shown in Table III. To render the experiment more practical, we incorporate load shedding into the analysis, with the penalty cost for load shedding set to be 10 times the energy purchase cost.

It is observed that the operation costs of RIES, EH1, and

EH2 obtained by the distributed robust optimization algorithm are marginally higher than those obtained by the distributed stochastic optimization algorithm. This is because the distributed stochastic optimization algorithm considers the operation cost in each scenario, while the distributed robust optimization algorithm solely considers the worst-case scenarios. Consequently, the distributed robust optimization algorithm is more conservative, but entails higher operation costs. At the same time, the distributed robust optimization algorithm involves lower operation risk and the cost of load shedding is much lower than that of the distributed stochastic optimization algorithm. Therefore, the total dispatch cost of the distributed robust optimization algorithm is lower than that of the distributed stochastic optimization algorithm.

TABLE III

COMPARISON OF RESULTS USING DISTRIBUTED ROBUST OPTIMIZATION AND DISTRIBUTED STOCHASTIC OPTIMIZATION ALGORITHMS

Algorithm	Cost (¥)					Total
	RIES	EH1	EH2	EH3	Load shedding	
Distributed robust optimization	74380	1040	930	480	21790	98620
Distributed stochastic optimization	73260	1030	920	540	27630	103380

C. Analysis of Centralized and Distributed Optimization Results

The centralized optimization model and the proposed model with initial step sizes ρ of 1, 3-7, 10, and 40 are solved, and the results are shown in Table IV. The results obtained using the proposed model align with those from the centralized optimization model across various step sizes. This agreement indicates that the proposed model attains the optimal operation results, achieving the integrated optimization of electric-gas-heat RIES and EHs as well as the autonomous decision-making of each subject. In addition, the number of iterations and computation time required for distributed optimization fluctuate with different initial step sizes. The step size of 4 yields fewer iterations and shorter convergence time, while step sizes below or above 4 lead to gradually slowing convergence. Therefore, selecting an appropriate step size can yield superior results.

The dispatch center under centralized optimization manages the system including the PDN, GDN, TDN, and EH, which is infeasible under practical engineering conditions. However, distributed optimization allows the regional system operator to optimize the PDN, GDN, and TDN dispatch, while EH operators optimize the dispatch of EH. This approach reduces the information interaction and communication demand. Using the proposed model with the step size of 4, the cost convergence curves of the electricity-gas-heat IES and EHs are shown in Fig. 10. At the beginning of the iteration, the cost of each sub-region shows a considerable change. However, by receiving information from neighboring sub-regions, each region adjusts its power allocation to achieve the overall balance of the IES.

TABLE IV

RESULTS OF CENTRALIZED OPTIMIZATION MODEL AND PROPOSED MODEL

Model	ρ	RIES cost (¥)	EH1 cost (¥)	EH2 cost (¥)	EH3 cost (¥)	Total cost (¥)	Number of iterations	Computation time (s)
Centralized		83540	1070	970	540	86120		155
Proposed	1	83540	1070	970	540	86120	32	825
	3	83540	1070	970	540	86120	34	799
	4	83540	1070	970	540	86120	26	637
	5	83540	1070	970	540	86120	29	696
	6	83540	1070	970	540	86120	32	765
	7	83540	1070	970	540	86120	32	772
	10	83540	1070	970	540	86120	40	965
40	83540	1070	970	540	86120	38	1233	

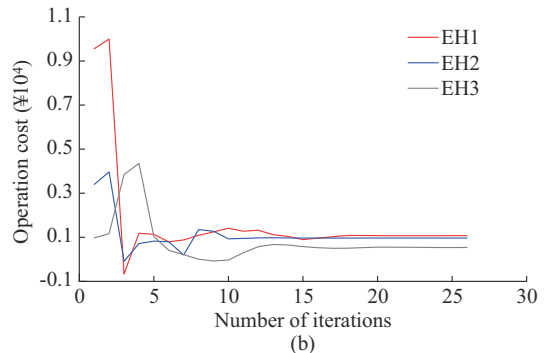
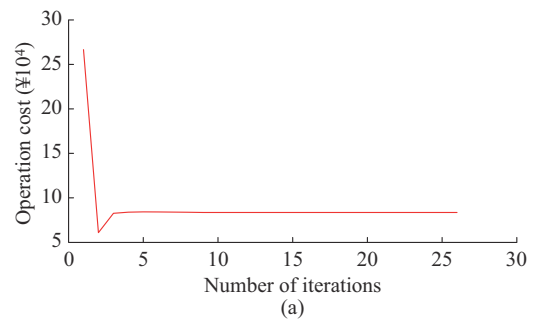


Fig. 10. Cost convergence curves of electricity-gas-heat IES and EHs using proposed model. (a) Operation cost of electricity-gas-heat IES. (b) Operation cost of EHs.

D. Analysis of Convergence of ADMM with Adaptive Step Size

Table V illustrates the performance of the traditional ADMM algorithm and ADMM algorithm with adaptive step size for initial step sizes of 1, 4, and 40. When $\rho=4$, the computational efficiency of the ADMM algorithm with adaptive step size aligns closely with that of the traditional ADMM algorithm. However, when $\rho=1$ or $\rho=40$, the ADMM algorithm with adaptive step size demonstrates significantly superior performance than the traditional ADMM algorithm, with results similar to those with step size of $\rho=4$. This improvement stems from the ADMM algorithm with adaptive step size could automatically adjust the step size based on the relationship between the residuals at various initial step sizes, which makes the convergence more stable.

TABLE V
RESULTS OF TRADITIONAL ADMM ALGORITHM AND ADMM ALGORITHM
WITH ADAPTIVE STEP SIZE

Algorithm	ρ	Number of iterations	Computation time (s)
Traditional ADMM	1	70	1857
	4	33	847
	40	163	3705
ADMM with adaptive step size	1	32	825
	4	26	637
	40	38	1233

Figure 11 illustrates the convergence curves of dual and original residual values of both algorithms using an initial step size of 1. Both algorithms exhibit a similar convergence trend. However, traditional ADMM algorithm exhibits slow convergence of the original and dual residuals during $[0, 1]$, with values dropping by merely 0.052414 and 0.008866 in the last 40 iterations. In contrast, for the ADMM algorithm with adaptive step size, only 33 iterations are necessary, which solves the problem of low convergence efficiency caused by the suboptimal initial step size settings of traditional ADMM algorithms.

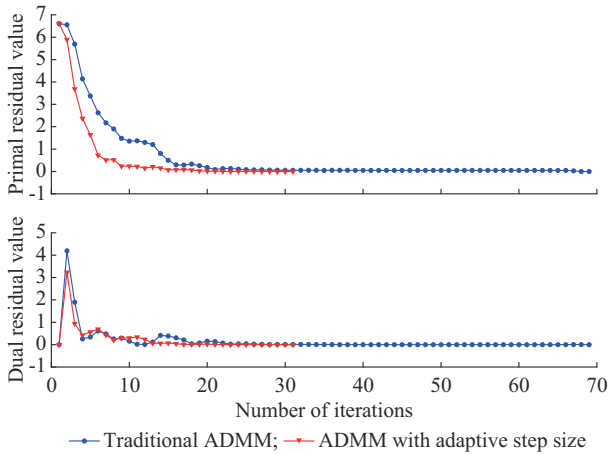


Fig. 11. Convergence curves of dual and original residual values of two algorithms using an initial step size of 1.

V. CONCLUSION

This paper proposes a distributed robust optimal dispatch model of RIES, taking into account the distribution network and each EH as independent operators. Robust optimization is employed within each operator to improve the operation security in cases of wind and PV power output uncertainties, with only deterministic information exchanged at the boundaries. In addition, the ADMM algorithm is implemented for the distributed optimization operation of the multi-energy RIES, maximizing the operational data safety and benefits for each entity. Furthermore, the traditional ADMM algorithm with fixed step size is modified to an ADMM algorithm with adaptive step size, effectively mitigating excessive information exchanges between operators resulting from suboptimal step size settings. The validity of the proposed model is validated using an example system, yielding the fol-

lowing results: ① the robust optimization entails higher operation costs than stochastic optimization, the latter results in a more significant load reduction in post-decision, which means that robust optimization costs less; ② the ADMM algorithm with adaptive step size achieves identical dispatch results as the centralized optimization algorithm. However, when the initial step size setting is suboptimal, it outperforms the traditional one. Therefore, the proposed model offers a new solution to the optimal dispatch issue of RIES involving various stakeholders. Future research will focus on energy sharing among EHs.

REFERENCES

- [1] T. Nakata, D. Silva, and M. Rodionov, "Application of energy system models for designing a low-carbon society," *Progress in Energy and Combustion Science*, vol. 37, no. 4, pp. 462-502, Aug. 2011.
- [2] D. Wang, L. Liu, H. Jia *et al.*, "Review of key problems related to integrated energy distribution systems," *CSEE Journal of Power and Energy Systems*, vol. 4, no. 2, pp. 130-145, Jun. 2018.
- [3] C. Yan, Z. Bie, S. Liu *et al.*, "A reliability model for integrated energy system considering multi-energy correlation," *Journal of Modern Power Systems and Clean Energy*, vol. 9, no. 4, pp. 811-825, Jul. 2021.
- [4] Carmen. (2022, Aug.). RS cogeneration plant, US. [Online]. Available: <https://www.power-technology.com/marketdata/rs-cogeneration-plant-us/>
- [5] AOC. (2018, Aug.). Cogeneration at the Capitol power plant. [Online]. Available: <https://www.aoc.gov/what-we-do/projects/cogeneration-capitol-power-plant>
- [6] C. EUROPE. (2023, Aug.). Cogeneration in 2050. [Online]. Available: <https://www.cogeneurope.eu/knowledge-centre/cogeneration-in-2050>
- [7] C. S. T. Alliance. (2018, Aug.). National Science and Technology Support Project of Tianjin University "Demonstration of Multi-energy Complementary Heating System Integrated with Buildings" passed the acceptance test. [Online]. Available: <http://www.cnste.org/html/jiaodian/2018/0426/3015.html>
- [8] Z. Cao, Q. Zhao, J. Wang *et al.*, "Edge-cloud collaborative architecture based multi-time scales rolling optimization of regional integrated electrical and natural gas energy system considering wind power uncertainty," *IET Generation, Transmission & Distribution*, vol. 15, no. 19, pp. 2684-2709, Oct. 2021.
- [9] J. Gao, Y. Yang, F. Gao *et al.*, "Two-stage robust economic dispatch of regional integrated energy system considering source-load uncertainty based on carbon neutral vision," *Energies*, vol. 15, no. 4, p. 1596, Feb. 2022.
- [10] L. Sun and F. You, "Machine learning and data-driven techniques for the control of smart power generation systems: an uncertainty handling perspective," *Engineering*, vol. 7, no. 9, pp. 1239-1247, Sept. 2021.
- [11] J. Zhai, X. Wu, S. Zhu *et al.*, "Low carbon economic dispatch of regional integrated energy system considering load uncertainty," in *Proceedings of 2019 34th Youth Academic Annual Conference of Chinese Association of Automation (YAC)*, Jinzhou, China, Jun. 2019, pp. 642-647.
- [12] X. Shen, Q. Guo, Y. Xu *et al.*, "Robust planning method for regional integrated energy system considering multi-energy load uncertainties," *Automation of Electric Power Systems*, vol. 43, no. 7, pp. 34-41, Apr. 2019.
- [13] L. Ge, Y. Li, J. Yan *et al.*, "Short-term load prediction of integrated energy system with wavelet neural network model based on improved particle swarm optimization and chaos optimization algorithm," *Journal of Modern Power Systems and Clean Energy*, vol. 9, no. 6, pp. 1490-1499, Nov. 2021.
- [14] Y. Zhou, Z. Wei, G. Sun *et al.*, "A robust optimization approach for integrated community energy system in energy and ancillary service markets," *Energy*, vol. 148, pp. 1-15, Apr. 2018.
- [15] L. Ji, B. Zhang, G. Huang *et al.*, "Robust regional low-carbon electricity system planning with energy-water nexus under uncertainties and complex policy guidelines," *Journal of Cleaner Production*, vol. 252, p. 119800, Apr. 2020.
- [16] X. Song, R. Zhao, G. De *et al.*, "A fuzzy-based multi-objective robust optimization model for a regional hybrid energy system considering uncertainty," *Energy Science & Engineering*, vol. 8, no. 4, pp. 926-943, Apr. 2020.

- [17] Y. Lei, D. Wang, H. Jia *et al.*, "Multi-stage stochastic planning of regional integrated energy system based on scenario tree path optimization under long-term multiple uncertainties," *Applied Energy*, vol. 300, p. 117224, Oct. 2021.
- [18] W. Liang, S. Lin, M. Liu *et al.*, "Stochastic economic dispatch of regional integrated energy system considering the pipeline dynamics using improved approximate dynamic programming," *International Journal of Electrical Power & Energy Systems*, vol. 141, p. 108190, Oct. 2022.
- [19] H. Liu, Z. Fan, H. Xie *et al.*, "Distributionally robust joint chance-constrained dispatch for electricity-gas-heat integrated energy system considering wind uncertainty," *Energies*, vol. 15, no. 5, p. 1796, Feb. 2022.
- [20] Y. Wang, Y. Wang, Y. Huang *et al.*, "Optimal scheduling of the regional integrated energy system considering economy and environment," *IEEE Transactions on Sustainable Energy*, vol. 10, no. 4, pp. 1939-1949, Oct. 2019.
- [21] Z. Guo, R. Zhang, L. Wang *et al.*, "Optimal operation of regional integrated energy system considering demand response," *Applied Thermal Engineering*, vol. 191, p. 116860, Jun. 2021.
- [22] X. Chen, M. B. McElroy, and C. Kang, "Integrated energy systems for higher wind penetration in China: formulation, implementation, and impacts," *IEEE Transactions on Power Systems*, vol. 33, no. 2, pp. 1309-1319, Mar. 2018.
- [23] L. Liu, D. Wang, K. Hou *et al.*, "Region model and application of regional integrated energy system security analysis," *Applied Energy*, vol. 260, p. 114268, Feb. 2020.
- [24] Y. Wang, Y. Wang, Y. Huang *et al.*, "Operation optimization of regional integrated energy system based on the modeling of electricity-thermal-natural gas network," *Applied Energy*, vol. 251, p. 113410, Oct. 2019.
- [25] Y. Zhou, Z. Wei, M. Shahidehpour *et al.*, "Distributionally robust resilient operation of integrated energy systems using moment and Wasserstein metric for contingencies," *IEEE Transactions on Power Systems*, vol. 36, no. 4, pp. 3574-3584, Jul. 2021.
- [26] J. Lu, T. Liu, C. He *et al.*, "Robust day-ahead coordinated scheduling of multi-energy systems with integrated heat-electricity demand response and high penetration of renewable energy," *Renewable Energy*, vol. 178, pp. 466-482, Nov. 2021.
- [27] E. A. Martínez-Ceseña and P. Mancarella, "Energy systems integration in smart districts: robust optimisation of multi-energy flows in integrated electricity, heat and gas networks," *IEEE Transactions on Smart Grid*, vol. 10, no. 1, pp. 1122-1131, Jan. 2019.
- [28] L. Strezoski, H. Padullaparti, F. Ding *et al.*, "Integration of utility distributed energy resource management system and aggregators for evolving distribution system operators," *Journal of Modern Power Systems and Clean Energy*, vol. 10, no. 2, pp. 277-285, Mar. 2022.
- [29] Z. Yi, Y. Xu, J. Hu *et al.*, "Distributed, neurodynamic-based approach for economic dispatch in an integrated energy system," *IEEE Transactions on Industrial Informatics*, vol. 16, no. 4, pp. 2245-2257, Apr. 2020.
- [30] Q. Peng, X. Wang, Y. Kuang *et al.*, "Hybrid energy sharing mechanism for integrated energy systems based on the Stackelberg game," *CSEE Journal of Power and Energy Systems*, vol. 7, no. 5, pp. 911-921, Sept. 2021.
- [31] Y. Tao, J. Qiu, S. Lai *et al.*, "Integrated electricity and hydrogen energy sharing in coupled energy systems," *IEEE Transactions on Smart Grid*, vol. 12, no. 2, pp. 1149-1162, Mar. 2021.
- [32] Z. Yang, J. Hu, X. Ai *et al.*, "Transactive energy supported economic operation for multi-energy complementary microgrids," *IEEE Transactions on Smart Grid*, vol. 12, no. 1, pp. 4-17, Jan. 2021.
- [33] J. Wei, Y. Zhang, J. Wang *et al.*, "Decentralized demand management based on alternating direction method of multipliers algorithm for industrial park with CHP units and thermal storage," *Journal of Modern Power Systems and Clean Energy*, vol. 10, no. 1, pp. 120-130, Jan. 2022.
- [34] N. Jia, C. Wang, W. Wei *et al.*, "Decentralized robust energy management of multi-area integrated electricity-gas systems," *Journal of Modern Power Systems and Clean Energy*, vol. 9, no. 6, pp. 1478-1489, Nov. 2021.
- [35] W. Fan, L. Ju, Z. Tan *et al.*, "Two-stage distributionally robust optimization model of integrated energy system group considering energy sharing and carbon transfer," *Applied Energy*, vol. 331, p. 120426, Feb. 2023.
- [36] X. Zhang, Z. Liang, and S. Chen, "Optimal low-carbon operation of regional integrated energy systems: a data-driven hybrid stochastic-distributionally robust optimization approach," *Sustainable Energy, Grids and Networks*, vol. 34, p. 101013, Jun. 2023.
- [37] P. Wang, Q. Wu, S. Huang *et al.*, "ADMM-based distributed active and reactive power control for regional AC power grid with wind farms," *Journal of Modern Power Systems and Clean Energy*, vol. 10, no. 3, pp. 588-596, May 2022.
- [38] H. G. Yeh, D. F. Gayme, and S. H. Low, "Adaptive VAR control for distribution circuits with photovoltaic generators," *IEEE Transactions on Power Systems*, vol. 27, no. 3, pp. 1656-1663, Aug. 2012.
- [39] S. Chen, Z. Wei, G. Sun *et al.*, "Adaptive robust day-ahead dispatch for urban energy systems," *IEEE Transactions on Industrial Electronics*, vol. 66, no. 2, pp. 1379-1390, Feb. 2019.
- [40] A. S. Gaur, D. Z. Fitiwi, and J. Curtis, "Heat pumps and our low-carbon future: a comprehensive review," *Energy Research & Social Science*, vol. 71, p. 101764, Jan. 2021.
- [41] J. Eckstein and M. Fukushima, "Some reformulations and applications of the alternating direction method of multipliers," in *Large Scale Optimization: State of the Art*. Dordrecht: Kluwer Academic Publishers, 1993, pp. 115-134.
- [42] S. Boyd, "Distributed optimization and statistical learning via the alternating direction method of multipliers," *Foundations and Trends in Machine Learning*, vol. 3, no. 1, pp. 1-122, Aug. 2010.
- [43] Y. Qiu, S. Lu, H. Lu *et al.*, "Flexibility of integrated energy system: basic connotation, mathematical model and research framework," *Automation of Electric Power Systems*, vol. 46, no. 17, pp. 16-43, Sept. 2022.
- [44] S. Chen, A. J. Conejo, R. Sioshansi *et al.*, "Investment equilibria involving gas-fired power units in electricity and gas markets," *IEEE Transactions on Power Systems*, vol. 35, no. 4, pp. 2736-2747, Jul. 2020.
- [45] X. Liu, J. Wu, N. Jenkins *et al.*, "Combined analysis of electricity and heat networks," *Applied Energy*, vol. 162, pp. 1238-1250, Jan. 2016.
- [46] P. Pinson, "Wind energy: forecasting challenges for its operational management," *Statistical Science*, vol. 28, no. 4, pp. 1238-1250, Nov. 2013.
- [47] L. A. Barroso and A. J. Conejo, "Decision making under uncertainty in electricity markets," in *Proceedings of 2006 IEEE PES General Meeting*, Montreal, Canada, Jul. 2006, pp. 1-3.

Zhoujun Ma received the B.S. degree in electrical engineering from Southeast University, Nanjing, China, in 2009, and the M.S. degree in Shanghai Jiao Tong University, Shanghai, China, in 2013. He is currently pursuing the Ph.D. degree in Hohai University, Nanjing, China. His research interests include power distribution dispatch, operation, and control of power system.

Yizhou Zhou received the B.S. and Ph.D. degrees in electrical engineering from Hohai University, Nanjing, China, in 2015 and 2020, respectively. He was a Visiting Scholar from October 2018 to October 2019 with the Illinois Institute of Technology, Chicago, USA. He is now a Lecturer with the College of Energy and Electrical Engineering, Hohai University. His research interests include integrated energy system, power system operation and planning, and electricity market.

Yuping Zheng received the B.S. degree from Hefei University of Technology, Hefei, China, in 1983, the M.S. degree from Nanjing Automation Research Institute, Nanjing, China, in 1986, and the Ph.D. degree from Wuhan University, Wuhan, China, in 2004. His research interests include relay protection and control of AC/DC hybrid power system.

Li Yang received the B.S. degree from the College of Energy and Electrical Engineering, Hohai University, Nanjing, China, in 2020. He is currently pursuing the M.S. degree in electrical engineering with the College of Energy and Electrical Engineering, Hohai University. His research interests include electric-gas integrated energy system and integration of renewable energy sources.

Zhinong Wei received the B.S. degree from Hefei University of Technology, Hefei, China, in 1984, the M.S. degree from Southeast University, Nanjing, China, in 1987, and the Ph.D. degree from Hohai University, Nanjing, China, in 2004. He is currently a Professor of electrical engineering with the College of Energy and Electrical Engineering, Hohai University. His research interests include integrated energy system, power system state estimation, smart distribution system, and integration of distributed generation into electric power system.